Desalination and Water Treatment
www.deswater.com

doi:10.5004/dwt.2017.21518

93 (2017) 309–317
October

Green synthesis of clay/silver nanocomposite materials for adsorption of hazardous dyestuffs

Melike Oğuz, Hüseyin Usluer, Deniz Uzunoğlu, Ayla Özer

Mersin University, Chemical Engineering Department, Mersin, Turkey, email: m-oguz91@hotmail.com (M. Oğuz), huseyinusluerce@gmail.com (H. Usluer), denizuzunoglu4@gmail.com (D. Uzunoğlu), ayozer@mersin.edu.tr (A. Özer)

Received 9 March 2017; Accepted 2 October 2017

ABSTRACT

In this study, clay/silver nanocomposite material (clay/AgNCs) was biosynthesized using *Acacia cyanophylla* extract, and the synthesized clay/AgNCs material was used as an adsorbent for adsorption of the Methylene Blue (MB) and Telon Blue AGLF (TB) dyes, known as hazardous dyestuffs. The optimum initial pH, temperature, and adsorbent concentration were determined to be 8.0, 45°C, and 1.0 g/L for MB adsorption and 8.0, 55°C, and 1.0 g/L for TB adsorption, respectively. The experimental equilibrium data for MB and TB adsorption were fitted well to the Freundlich and Langmuir isotherm models, respectively. The studied adsorption process followed the pseudo second order kinetic model. Weber-Morris model results showed that both intraparticle and film diffusion were effective on the studied adsorption systems. The thermodynamic parameters showed that MB and TB adsorption on clay/AgNCs were endothermic, increasing in randomness of adsorbed species and spontaneous for MB adsorption, induced for TB adsorption. Moreover, clay/AgNCs were characterized by DLS, FT-IR, XRD, SEM and EDX analysis methods.

Keywords: *Acacia cyanophylla*; Adsorbent characterization; Dyestuff adsorption; Biosynthesis; Leaf extract; Nanocomposite

1. Introduction

Many investigations have been conducted on physico-chemical methods of removing colorful effluents, which include the use of coagulants, oxidizing agents, ultra-filtration, electro-chemistry, and adsorption. Most of these methods have limitations such as high capital and operational cost, low efficiency, sensitive operating conditions and production of secondary sludge. Adsorption by an eco-friendly adsorbent attracts attention as an economic and efficient method for water and wastewater treatment, especially dyestuff removal [1]. In recent years, there is a growing interest in the usage of metallic nanoparticles (MeNPs) as adsorbents for dyestuff removal because they have significant advantages such as only a little amount of nanomaterial is required for removing of the pollutants from aqueous solutions, their adsorption capacities are relatively high because of high specific surface area and also a large number of unsaturated atoms on their surfaces [2–4].

There are various methods for the synthesis of MeNPs, such as complex synthesis/reduction procedures, co-precipitation, microemulsion, sonochemical, and photochemical techniques, but most of them are environmentally unfriendly and expensive. MeNPs are frequently prepared by chemical methods involving reducing agents, hydrazine hydrate, sodium boro-hydride, ethylene glycol, etc., which are very much hazardous to the environment. Thus, synthesis of MeNPs by living organisms such as bacteria, algae, fungi, and plants are currently paid more attention. The using plant extract is more suitable due to its simplicity, cost efficiency, eco-friendliness, and production of more stable nanoparticles in comparison with the using microorganisms [5]. Given the diversity of plants in our country; plant leaves, unused eco-friendly resources, can be converted into economic value when they are evaluated in metallic nanoparticles biosynthesis. Also, the preparation of metal-

*Corresponding author.

Presented at the 3rd International Conference on Recycling and Reuse, 28-30 September 2016, Istanbul, Turkey

1944-3994 / 1944-3986

lic nanocomposites based on natural materials such as clay minerals, biopolymers has lately attracted much attention in many application areas due to their cost efficiency, unique structure, and properties. These metallic nanocomposite materials can combine the properties of both inorganic and organic components, such as mechanical properties, water uptake, swelling, rheology, adhesion, and thermal behavior [6]. Biobased metallic nanocomposites are cost-effective and environment-friendly materials for the wastewater treatment applications. In this regard, some of MeNPs have also been synthesized in natural materials, which have two-dimensional interlayer space, intercalation, swelling, and ion exchange properties. Its interlayer space is used for the synthesis of MeNPs, as support for anchoring transition-metal complex catalysts, and as adsorbents for various ions [7]. In this respect, clay/silver nanocomposite material (clay/AgNCs) were biosynthesized using *Acacia cyanophylla* extract, and used as adsorbent for adsorption of the methylene blue (MB) and Telon Blue AGLF (TB) from aqueous solutions in this work. An innovative aspect of our research is the first time use of biosynthesized metallic nanocomposite material with unique compounds in the dye adsorption system. The equilibrium, kinetic, and mass transfer modelling of the adsorption of MB and TB onto clay/AgNCs was also performed.

2. Material and methods

2.1. Biosynthesis of clay/AgNCs nanocomposite material

Fresh leaves of *Acacia cyanophylla* were washed with distilled water to purify of impurities and then dried in an oven at 110°C. *A. cyanophylla* leaf extract (LEx) was prepared by boiling 5.0 g of the dried leaves in 100 mL of distilled water at 100°C for 120 min. The extract was centrifuged to remove insoluble fractions and macromolecules. Lastly, the obtained dark yellow extract was stored in the refrigerator for further the synthesis experiments. For clay/AgNCs synthesis; 100 mL of 10^{-3} M $AgNO_3$ was firstly mixed with 0.02 g of clay, and then 5.0 mL of LEx at room temperature as natural reductant was dropped by syringe pump to the prepared $AgNO_3$-clay mixture. The formation of clay/AgNCs was confirmed when the color of the solution started to convert from transparent color to dark brown. The filtrate was washed comprehensively with distilled water and then was dried at 110°C in an oven for 24 h. The clay/AgNCs were ground homogeneously by mortar and were stored in closed vessels in a refrigerator for the adsorption experiments [8]. Synthesized clay/AgNCs were characterized by DLS, FT-IR, XRD, SEM and EDX analysis methods.

2.2. Adsorption experiments

The adsorption experiments with artificial wastewater of TB ($C_{37}H_{38}N_5NaO_6S_2$) and MB ($C_{16}H_{18}ClN_3S$) on clay/AgNCs were done in a batch system. 0.1 g of clay/AgNCs, except for adsorbent concentration experiments, was mixed with 100 mL of the desired initial dye concentration and initial pH in 250 mL-Erlenmeyer flasks. The flasks were agitated on a shaker with 600 rpm shaking speed at constant temperature for 180 min to obtain adsorption equilibrium. Samples were taken before mixing the adsorbent and dyestuff-bearing solution, then at predetermined time intervals (in the range of 0.5–180 min) for the residual dyestuff concentration in the solution. They were separated from the adsorbent with centrifuge at 3000 rev/min for 5 min. The unadsorbed TB and MB concentrations in supernatant were analyzed at 610 nm and 662 nm, respectively, with Chebios brand UV–vis spectrophotometer. Experiments were repeated for different initial pH, initial dye concentration, temperature and adsorbent concentration values.

The adsorbed amount at equilibrium, q_e (mg/g), and the percentage of adsorption (%) were computed as follows:

$$Q_e = (C_o - C_e)/X_o \quad (1)$$

$$\text{Percent adsorption (\%)} = ((C_o - C_e)/C_o) \times 100 \quad (2)$$

3. Results and discussion

3.1. Characterizations of clay/AgNCs

The distribution of effective hydrodynamic diameters of clay/AgNCs was measured by DLS technique and the results are presented in Fig. 1. As can be seen from Fig. 1, the average particle size of biosynthesized clay/AgNCs was determined as 114.6 nm with low polydispersity index (PDI) of 0.363.

In order to determine the functional groups of clay/AgNCs, FT-IR spectrums of clay/AgNCs before and after adsorption were recorded and they were presented in Fig. 2. Accordingly, the bands at 1622, 1373, and 1031 cm^{-1} corresponded to the peak of –COOH carbonyl group, C-N stretching vibrations of aromatic amine, and characteristic of C-OH stretching of secondary alcohols, respectively. These data showed the presence of carbonyls, amine groups, and amino acid residues present in LEx in clay/AgNCs synthesis. The characteristic peaks of aromatic phenols at 800–500 cm^{-1} region (for C-H out of plane bend) are also observed in Fig. 2 [9]. Moreover, the characteristic bands of clay content were determined at 1031 cm^{-1} for Si-O in-plane stretch-

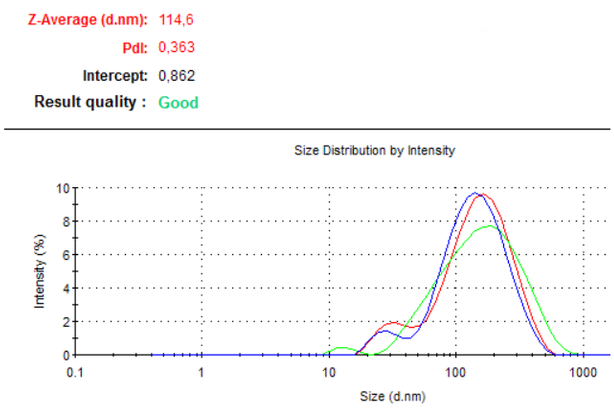

Fig. 1. The distribution of effective hydrodynamic diameters of clay/AgNCs.

ing, 920 cm^{-1} for Al-OH-Al bending, and 796 cm^{-1} for Al-O stretching [10].

The crystal structure of clay/AgNCs was determined by using XRD analysis method. XRD patterns of clay/AgNCs before and after adsorption are shown in Fig. 3. XRD pattern of the clay/AgNCs exhibited peaks at 2θ angles of 38.10°, 44.28°, 64.50°, and 77.42°which correspond to the [1 1 1], [2 0 0], [2 2 0], and [3 1 1] crystal planes of a cubic lattice structure of clay/AgNCs, respectively [11]. XRD pattern also revealed the presence of quartz, aluminosilicate, and feldspar phases related to clay [12].

Furthermore, it was observed that FTIR spectrums and XRD patterns of the clay/AgNCs before and after adsorption did not exhibit any differences, which was indicating physical adsorption processes.

The morphology investigation and elemental analysis of clay/AgNCs were performed by SEM and EDX, respectively and SEM images of clay/AgNCs with EDX spectrums before and after adsorption are presented in Fig. 4. Accordingly, the relatively porous and agglomerated structures were observed pre-adsorption, and these pores were covered by dyestuff molecules post-adsorption.

EDX analysis results are tabulated in Table 1. As can be seen from Table 1, the clay/AgNCs material before adsorp-

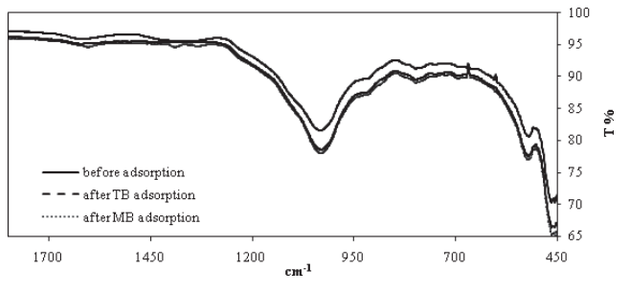

Fig. 2. FT-IR spectrums of clay/AgNCs before and after adsorption.

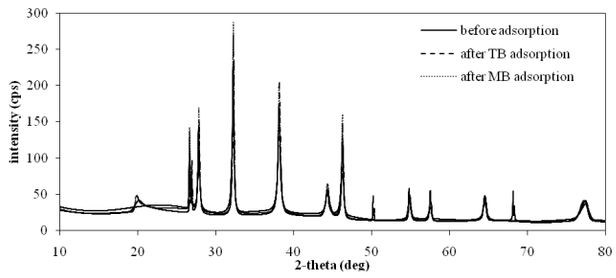

Fig. 3. XRD patterns of clay/AgNCs before and after adsorption.

Table 1
EDX analysis results

Element	% weight		
	Before adsorption	After MB adsorption	After TB adsorption
Ag	22.9	22.0	22.1
C	18.3	20.5	20.7
O	32.4	32.8	33.1
Si	19.6	18.2	18.1
Al	4.9	4.2	4.1
Fe	1.4	1.2	1.1
Mg	0.5	0.4	0.3
S	–	0.3	0.15
N	–	0.4	0.25
Na	–	–	0.1

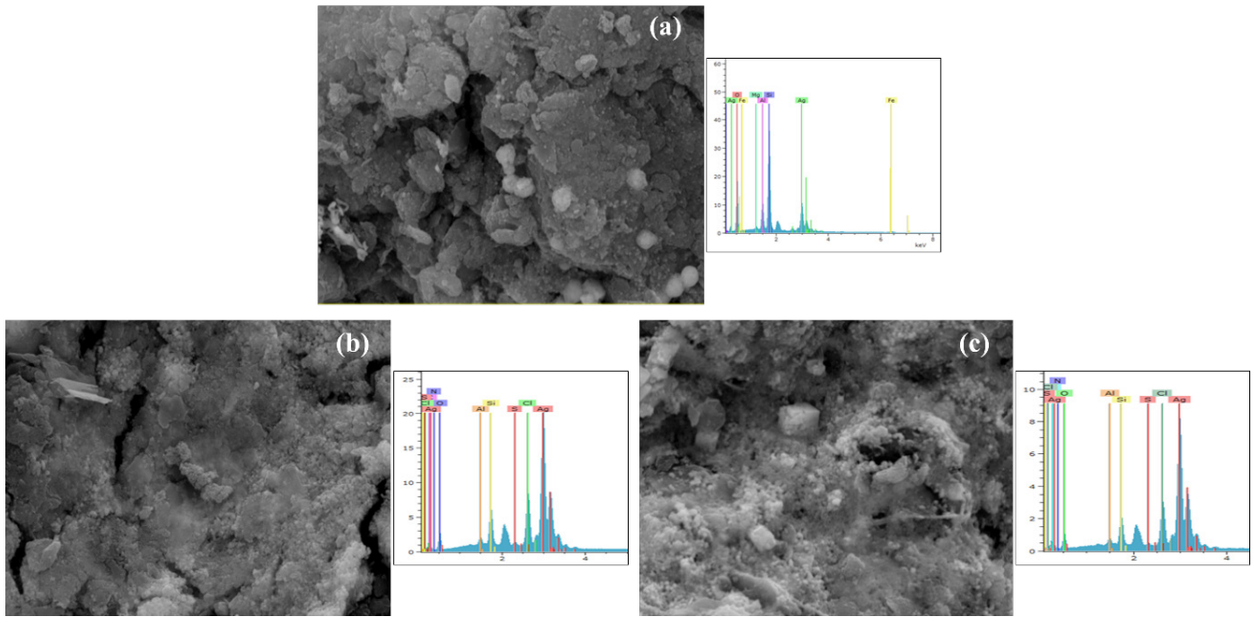

Fig. 4. SEM images of clay/AgNCs (a) before adsorption, (b) after TB adsorption, (c) after MB adsorption.

tion involved 32.4% O, 22.9% Ag, 19.6% Si, 18.3% C, 4.9% Al, 1.4% Fe, and 0.5% Mg. These results revealed the strong signal in the silver region and confirmed the formation of nanocomposite containing silver, and the determination of Si, Al, Mg peaks in EDX spectrum pre-adsorption indicated the presence of clay. The spectral signals for carbon, oxygen, and nitrogen also indicated that the extracellular bio-organic moieties from *A. cyanophylla* extract were also adsorbed on the surface of clay/AgNCs during the biosynthesis. In addition, the increasing in the percentages of carbon and the new formations 0.3% S and 0.4% N after MB ($C_{16}H_{18}ClN_3S$) adsorption; 0.15% S, 0.25% N, and 0.1% Na after TB ($C_{37}H_{38}N_5NaO_6S_2$) adsorption were observed resulting from the adsorbed dye molecules onto clay/AgNCs.

3.2. Effects of environmental conditions on the adsorption

The effects of environmental conditions such as initial pH, initial dye concentration, adsorbent concentration and temperature on adsorption of TB and MB dyestuffs by clay/AgNCs are shown in Figs. 5–9.

From Fig. 5a, it is observed that the maximum equilibrium uptake amounts (q_e) were observed at initial pH 8.0 and they decreased with increasing initial pH thereafter. In order to discuss the effect of initial pH; the zeta potential values of clay/AgNCs measured at different pH values (Fig. 5b) and the results show that the adsorbent surface was negatively charged at the initial pH range of 2.5–13.5. Accordingly, the maximum adsorption capacities of clay/AgNCs were observed at the maximum zeta potential value (–24.93 mV) of the adsorbent surface because maximum electrostatic attraction occurred between negatively charged adsorbent surface and cationic structure dyestuffs. The illustration about the electrostatic attraction is presented in Fig. 6. Besides, the negative charge of clay/AgNCs surface decreased at higher pH values than 8.0 and so the adsorbed amounts also decreased thereafter as a result of the decreasing in the mentioned electrostatic attraction. For

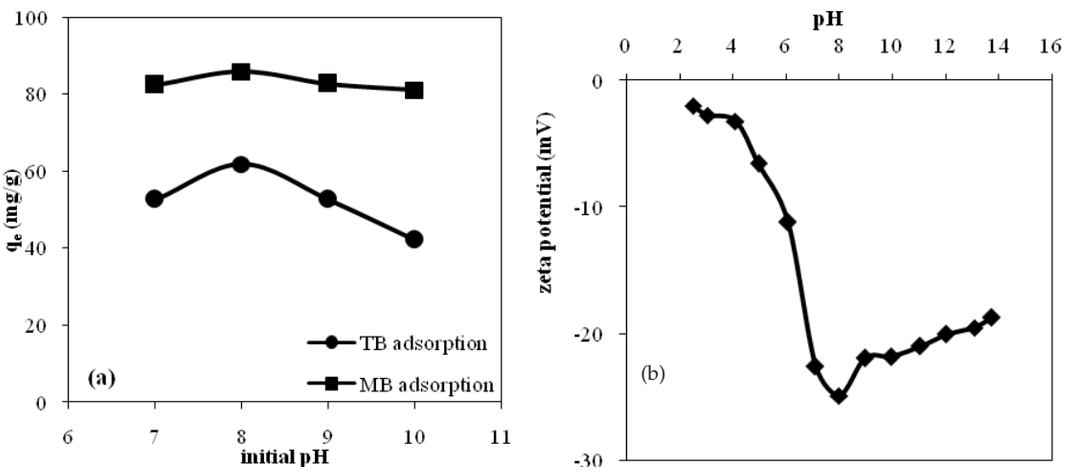

Fig. 5. (a) Effect of initial pH; (b) zeta potential values of clay/AgNCs for different pHs (C_o = 100 mg/L, T = 25°C, X_o = 1 g/L).

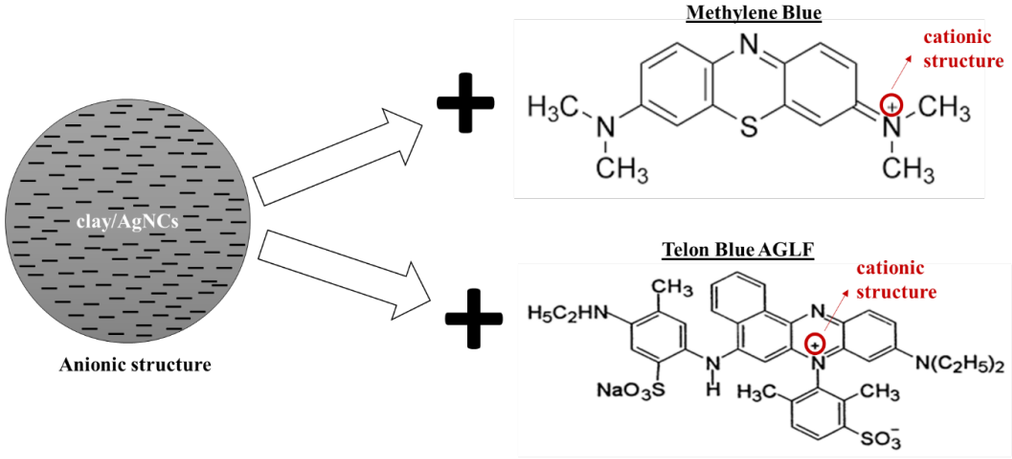

Fig. 6. The illustration about the electrostatic attraction between negatively charged adsorbent surface and cationic structure of dyestuffs.

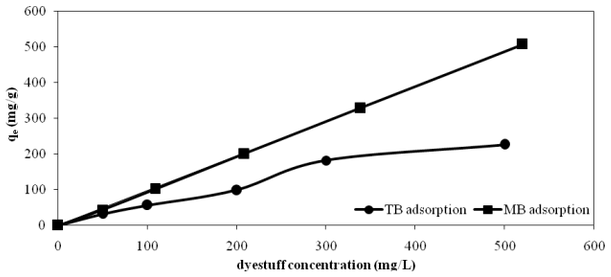

Fig. 7. Effect of initial dye concentration (initial pH = 8, T = 45°C, X_o = 1 g/L for MB adsorption; initial pH = 8, T = 55°C, X_o = 1 g/L for TB adsorption).

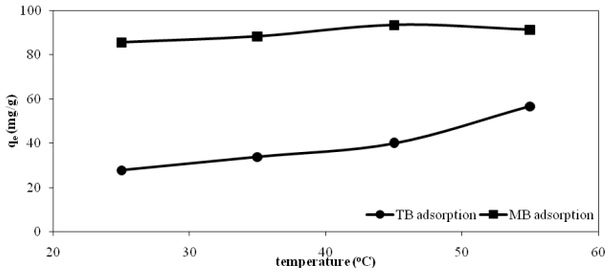

Fig. 8. Effect of temperature (initial pH = 8, C_o = 100 mg/L, X_o = 1 g/L for MB adsorption; initial pH = 8, C_o = 100 mg/L, X_o = 1 g/L for TB adsorption).

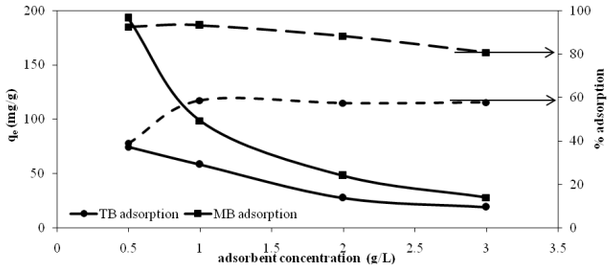

Fig. 9. Effect of adsorbent concentration (initial pH = 8, C_o = 100 mg/L, T = 45°C for MB adsorption; initial pH = 8, C_o = 100 mg/L, T = 55°C for TB adsorption).

these reasons, optimum initial pH values were found as 8.0 for MB and TB adsorption.

The prevenient mechanisms of TB and MB adsorption onto clay/AgNCs as follows;

$$TB^+ + COO^- \leftrightarrow [(TB^+)(COO^- Clay^-)] \quad Clay^- \tag{3}$$

$$MB^+ + COO^- \leftrightarrow [(MB^+)(COO^- Clay^-)] \quad Clay^- \tag{4}$$

According to Eqs. (3) and (4), cationic TB molecule ($[C_{37}H_{38}N_5NaO_3S]^+$) and MB molecule ($[C_{16}H_{18}N_3S]^+$) could adsorb onto carboxyl groups (COO^-) (indicated by FT-IR) and anionic clay structure.

Table 2
Thermodynamic parameters (initial pH = 8, C_o = 100 mg/L, X_o = 1 g/L)

Dyestuff	T (°C)	ΔH (J/mol)	ΔS (J/mol K)	ΔG (J/mol)
Telon Blue AGLF	25	65651.5	200.0	5983.5
	35			4252.2
	45			1762.1
	55			149.4
Methylene Blue	25	23054.7	91.9	-4399.6
	35			-5169.6
	45			-6245.6

The equilibrium uptake amounts along with the adsorption percentages for various initial dye concentrations are presented in Fig. 7. From Fig. 7, it was concluded that the equilibrium uptakes increased with increasing the initial TB concentration up to 300 mg/L and then slightly began to remain constant with further increase of initial TB concentration; on the other hand, the adsorption capacities increased linearly with increasing initial MB concentration in the studied dyestuff concentration ranges as a result of the increase in driving force (ΔC), which was giving the opportunity to work in the wide dyestuff concentration ranges.

The effect of temperature is shown in Fig. 8, the optimum temperature values for TB and MB adsorption were determined as 55°C and 45°C, respectively. Based on the results, the high adsorption capacities at high temperatures may be explained with the endothermic nature of the studied adsorption processes. This case was confirmed with thermodynamic parameters such as Gibb's free energy change (ΔG), enthalpy change (ΔH) and entropy change (ΔS) calculating by following equations [13]:

$$\ln(K_c) = (\Delta S/R) - (\Delta H/RT) \tag{4}$$

$$\Delta G = -RT \ln(K_c) \tag{5}$$

The calculated thermodynamic parameters are tabulated in Table 2. From Table 2, the studied adsorption systems were endothermic (ΔH>0), increasing in randomness of adsorbed species (ΔS>0), and induced (ΔG>0) for TB adsorption, spontaneous (ΔG<0) for MB adsorption.

Concentration and type of adsorbent are very important in adsorption systems because the adsorption take place on the active sites on surface and interior pores of the solid adsorbent. Thus, the effect of adsorbent concentration on the adsorption of TB and MB onto clay/AgNCs was studied for different adsorbent concentrations and the results are shown in Fig. 9. As can be seen from Fig. 9, the adsorption percentage increased up to 1.0 g/L of adsorbent concentration, and then slightly decreased with further increase in adsorbent concentration while the equilibrium uptakes decreased with increasing the adsorbent concentration. The aggregation of clay/AgNCs at high adsorbent concentrations may result in a decrease in the active surface area and an increase in the diffusional path length,

and so the lower adsorption capacities were observed at high adsorbent concentrations [14]. As a result, the optimum adsorbent concentration for MB and TB adsorption was determined as 1.0 g/L.

3.3. Equilibrium, kinetic, and mass transfer modelling

3.3.1. Equilibrium modelling

The well-known Langmuir and Freundlich isotherm models were applied to the experimental equilibrium data at different temperatures and the isotherm constants from the linearized isotherm equations and regression coefficients are summarized in Table 3. According to Table 3, MB adsorption equilibrium was described with the Freundlich isotherm model while the TB adsorption equilibrium was defined with the Langmuir isotherm model. Also, as it was expected that the maximum adsorption capacities were obtained at optimum temperature values. The increase of the adsorption capacities of clay/AgNCs with increasing temperature may be explained with the endothermic nature of the studied adsorption processes.

Besides, the experimental q_e and calculated q_e values from isotherm models vs C_e values at optimum temperatures are plotted in Fig. 10a and 10b. It was confirmed that the experimental equilibrium data of MB adsorption fitted to Freundlich isotherm model while the experimental equilibrium data of TB adsorption fitted Langmuir isotherm model in view of the isotherm model graphs in Fig. 10a and b.

The comparison of adsorption capacities of various nanocomposite types for various dye molecules in the literature is shown in Table 4. Accordingly, it can be seen that the nanocomposite used in this study has higher adsorption capacity in comparison to the other nanocomposite materials in the literature for dye adsorption.

3.3.2. Kinetic modelling

The adsorption kinetics of MB and TB onto clay/AgNCs were investigated by Lagergen's pseudo first order (PFOM) [$\log(q_e - q_t) = \log(q_e) - k_1 t/2.303$] and pseudo second order (PSOM) kinetic [$(t/q_t) = (1/q_e^2.k_2) + (t/q_e)$] models. The cal-

Table 3
The isotherm model constants with regression coefficient values (R^2) (initial pH = 8, X_o = 1 g/L)

Dye	T (°C)	Langmuir isotherm model [$q_e = Q°bC_e / (1+bC_e)$]			Freundlich isotherm model [$q_e = K_F C_e^{1/n}$]		
		Q_o (mg/g)	b (L/mg)	R^2	K_F (mg/g)/(L/mg)$^{1/n}$)	$1/n$	R^2
TB	25	78.64	0.00782	0.994	2.76	0.53	0.983
	35	82.50	0.01197	0.944	7.82	0.37	0.948
	45	716.33	0.00082	0.979	0.71	0.94	0.962
	55	1209.19	0.00108	0.991	1.55	0.94	0.978
MB	25	50.62	0.03013	0.892	33.85	2.91	0.986
	35	53.19	0.04003	0.895	49.26	3.14	0.987
	45	60.97	0.07018	0.898	54.63	3.74	0.987
	55	45.66	0.05883	0.878	41.19	3.50	0.985

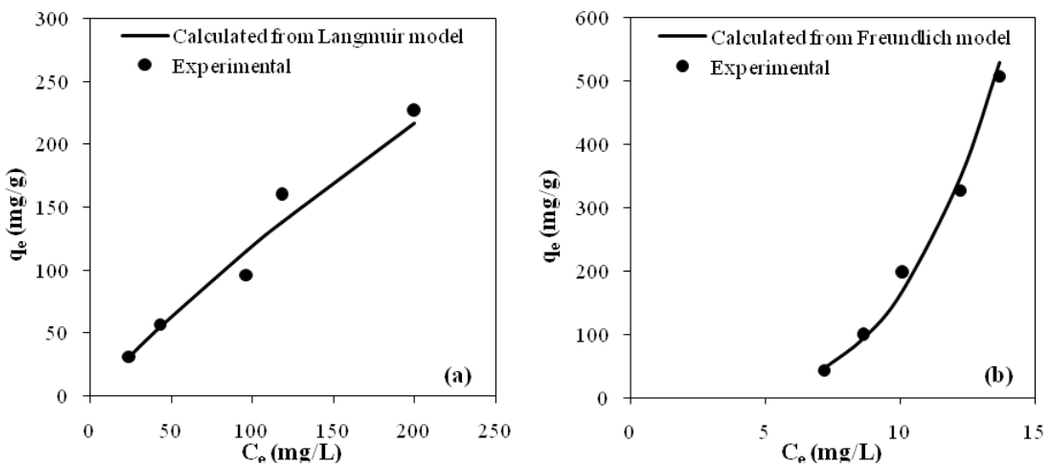

Fig. 10. The isotherm graphs (q_e vs. C_e) (a) TB adsorption (initial pH = 8, T = 55°C, X_o = 1 g/L); (b) MB adsorption (initial pH = 8, T = 45°C, X_o = 1 g/L).

Table 4
The comparison of adsorption capacities of various types of nanomaterials

Adsorbent	Size (nm)	Adsorbed dye	$Q_\circ$ (mg/g)	K_F ((mg/g)/(L/mg)$^{1/n}$)	Reference
NiO-Based nanomaterial	100	Telon Blue AGLF	370.37	–	[15]
Clay/AgNCs	114.6		1209.19	–	This study
Polyaniline zirconium (IV) silicophosphate nanocomposite	10–70		–	1.081	[16]
Goethite nanoadsorbent	22		–	8.96	[17]
Magnetite-loaded multi-walled carbon nanotubes	20–40	Methylene Blue	–	48.06	[18]
Poly(cyclotriphosphazene-co-4,4-sulfonyldiphenol) nanotubes	80		–	69.16	[19]
Clay/AgNCs	114.6		–	54.63	This study

Table 5
Kinetics and mass transfer model parameters with R^2 values (initial pH = 8, T = 45°C, X_o = 1 g/L for MB adsorption; initial pH = 8, T = 55°C, X_o = 1 g/L for TB adsorption)

Dye	C_o (mg/L)	$q_{e,exp}$ (mg/g)	Pseudo first order			Pseudo second order		
			k_1 (min^{-1})	$q_{e,cal1}$ (mg/g)	R^2	k_2 (g/(mg min))	$q_{e,cal2}$ (mg/g)	R^2
TB	55.5	32.2	0.02579	22.3	0.97	0.0044	32.9	0.99
	100.0	56. 7	0.02809	27.3	0.90	0.0056	57.1	0.99
	192. 8	96.1	0.02855	35.6	0.86	0.0048	96.5	0.99
	277. 8	181.7	0.03846	56.9	0.84	0.0035	182.8	0.99
	426.1	226.1	0.04260	53.1	0.66	0.0045	227.2	0.99
MB	50.3	43.1	0.0177	12.9	0.64	0.0071	42.3	0.99
	108.6	101.4	0.0263	26.3	0.79	0.0081	100.7	0.99
	208.6	199.9	0.0291	59.6	0.79	0.0032	199.1	0.99
	338.8	328.1	0.0403	115.5	0.85	0.0016	328.4	0.99
	520.1	506.4	0.0177	237.1	0.92	0.00066	503.8	0.99

culated rate constants and regression coefficients from the kinetic model plots ($\log(q_{eq} - q_t)$ vs. t for PFOM and t/q_t vs. t for PSOM; figures not shown) are summarized in Table 5 [20]. The consistency between the experimental and the calculated uptake values from the kinetic model plots is also presented in Fig. 11a and 11b. Accordingly, higher values of R^2 and the consistency between experimental and calculated uptake values showed excellent fit of the pseudo second order kinetics.

3.3.3. Effect of mass transfer

To evaluate the diffusion mechanism between dyestuff and clay/AgNCs, an intraparticle diffusion model proposed by Weber and Morris ($q_t = K_i \cdot t^{0.5} + I$) was used and the calculated parameters are presented in Table 6. Also, Weber–Morris plots are presented in Fig. 12a and 12b. Theoretically, if Weber–Morris plot of q_t vs. $t^{0.5}$ gives a straight line and pass through the origin, this means that only intraparticle diffusion controlled the adsorption process. On the other side, the Weber-Morris plot can be linear and also has intercept value if the adsorption system follows both intraparticle and film diffusion [21]. The plots of Weber-Morris model in Fig. 12(a) and (b) had three linear parts with different slopes, which indicated that more than one mechanism took place in the studied processes. Accordingly, the initial portion corresponded to the external diffusion, the second portion described the adsorption stage where intraparticle diffusion was effective on the process, and the third portion indicated the final equilibrium stage. Therefore, it was concluded from Table 6 and Fig. 12 that both intraparticle and film diffusion were effective on MB and TB adsorption processes.

4. Conclusions

In the present work, clay/silver nanocomposite material (clay/AgNCs) were synthesized by biosynthesis method using *Acacia cyanophylla* extract and the biosynthesized clay/AgNCs were characterized by DLS, FT-IR, XRD, SEM, and EDX analysis. The clay/AgNCs were eval-

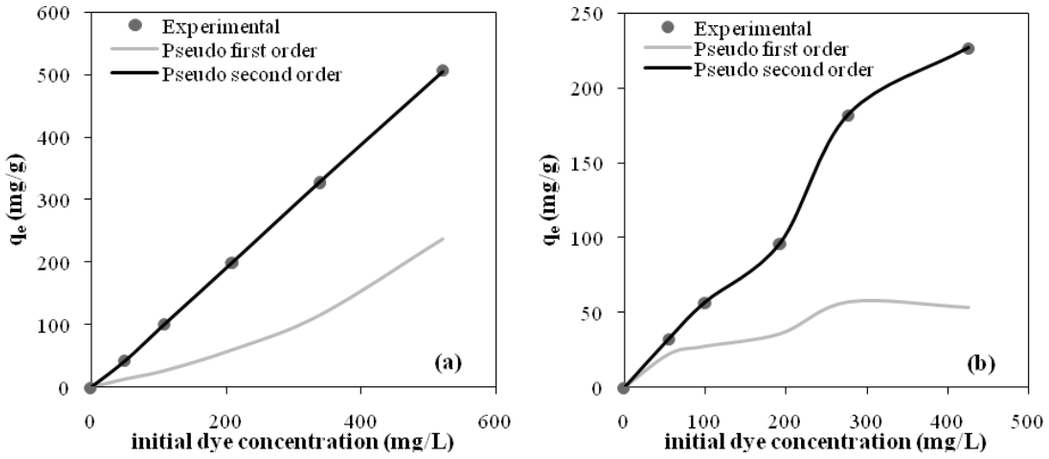

Fig. 11. The plots of the experimental and calculated adsorbed amounts at equilibrium vs. initial dye concentrations (a) MB adsorption (initial pH = 8, T = 45°C, X_o = 1 g/L); (b) TB adsorption (initial pH = 8, T = 55°C, X_o = 1 g/L).

Table 6
Kinetics and mass transfer model parameters with R^2 values (initial pH = 8, T = 45°C, X_o = 1 g/L for MB adsorption; initial pH = 8, T = 55°C, X_o = 1 g/L for TB adsorption)

Dye	C_o (mg/L)	$q_{e,exp}$ (mg/g)	K_i (mg/g.min$^{0.5}$)	Intercept	R^2
	55.5	32.2	2.7	7.6	0.96
	100.0	56. 7	4.9	21.8	0.95
TB	192. 8	96.1	5.1	55.7	0.97
	277. 8	181.7	6.9	126.8	0.97
	426.1	226.1	19.8	116.3	0.98
	50.3	43.1	14.1	6.28	0.99
	108.6	101.4	32.8	16.4	0.99
MB	208.6	199.9	49.5	26.6	0.94
	338.8	328.1	69.4	45.0	0.98
	520.1	506.4	103.9	58.1	0.97

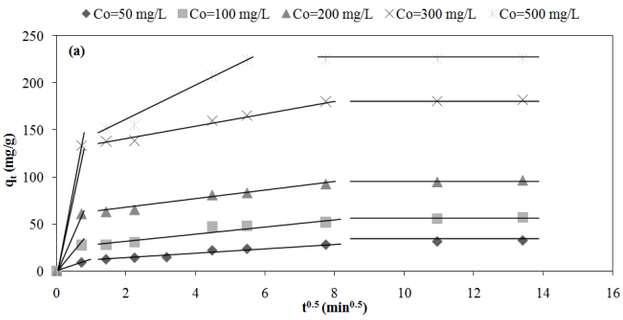

Fig. 12. (a) The plots of Weber-Morris intraparticle diffusion model for MB adsorption (initial pH = 8, T = 45°C, X_o = 1 g/L).

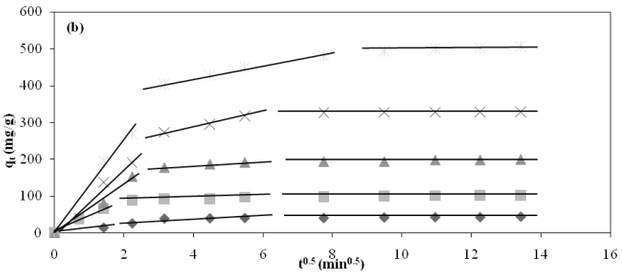

Fig. 12. (b) The plots of Weber-Morris intraparticle diffusion model for TB adsorption (initial pH = 8, T = 55°C, X_o = 1 g/L).

uated as potential adsorbents for removal of Methylene Blue (MB) and Telon Blue AGLF (TB) dyes from aqueous solutions in a single stage batch mode. The optimum initial pH, temperature, and adsorbent concentration were determined to be 8.0, 45°C, and 1.0 g/L for MB adsorption and 8.0, 55°C, and 1.0 g/L for TB adsorption, respectively. The equilibrium, kinetics, mass transfer modelling were also done. The kinetic modelling revealed that the pseudo second order kinetic model well-described the kinetic data of the adsorption of MB and TB onto clay/AgNCs rather than the pseudo first order model. Weber-Morris intraparticle diffusion model results showed that both intraparticle and film diffusion were effective on the studied adsorption systems. The experimental equilibrium data for MB and TB adsorption were fitted well to the Freundlich and Langmuir isotherm models, respectively. The maximum adsorption capacities at optimum temperature were determined as 1209.19 mg/g for TB and 54.63 mg/g for MB. These capacities were very high compared to the other adsorbents in the literature. It confirmed that clay/AgNCs may be used as effective adsorbents in small scale dyeing unit using batch or stirred-tank flow reactors and it can be concluded that it is enable to adsorb hazardous dyes by using one type adsorbent. Consequently, our findings open the possibility of biosynthesizing effective adsorbent by environmentally-friendly method for wastewater treatment applications. In addition, we suggest that novel nanocomposites with unique compounds can be biosynthesized by using different plant extract and the application areas can be extended by using the novel nanocomposites.

Symbols

b — A constant related to the affinity of the binding sites (L/mg)
C_e — Unadsorbed dyestuff concentration at equilibrium (mg/L)
C_o — Initial dyestuff concentration (mg/L)
K_c — Equilibrium constant
K_F — Freundlich constant indicating adsorption capacity ((mg/g)/(L/mg)$^{1/n}$)
K_i — Intraparticle diffusion rate constant (mg/g·min$^{1/2}$)
k_1 — Pseudo first order kinetic rate constant (1/min)
k_2 — Pseudo second order kinetic rate constant (g/mg·min)
I — intercept value of Weber-Morris plot
q_e — Adsorbed amount per unit mass of adsorbent (mg/g)
$q_{e,cal1}$ — Calculated adsorbed amount per unit mass of adsorbent from pseudo first order kinetic model (mg/g)
$q_{e,cal2}$ — Calculated adsorbed amount per unit mass of adsorbent from pseudo second order kinetic model (mg/g)
$q_{e,exp}$ — Experimental adsorbed amount per unit mass of adsorbent (mg/g)
q_t — Adsorbed amount per unit mass of adsorbent at any time (mg/g)
$Q_\circ$ — Maximum monolayer coverage capacity of adsorbent (mg/g)
X_o — Adsorbent concentration (g/L)
R — Ideal gas constant (J/molK)
R^2 — Regression coefficient
T — Temperature (°C, K)
t — Time (min)
ΔG — Change of Gibb's energy (J/mol)
ΔH — Change of enthalpy (J/mol)
ΔS — Change of entropy (J/molK)
$1/n$ — Freundlich constant indicating adsorption intensity

References

[1] E. Zeynep, F.N. Acar, Adsorption of Reactive Black 5 from an aqueous solution: equilibrium and kinetic studies, Desalination, 194 (2006) 1–10.
[2] A. Thirumurugan, P. Aswitha, C. Kiruthika, S. Nagarajan, A.N. Christy, Green synthesis of platinum nanoparticles using *Azadirachta indica*–An eco-friendly approach, Mater. Lett., 170 (2016) 175–178.
[3] C. Cao, L. Xiao, C. Chen, X. Shi, Q. Cao, L. Gao. In situ preparation of magnetic Fe_3O_4/chitosan nanoparticles via a novel reduction–precipitation method and their application in adsorption of reactive azo dye, Powder Technol., 260 (2014) 90–97.
[4] M.A. Ahmed, M.A. Messih, E.F. El-Sherbeny, S.F. El-Hafez, A.M. Khalifa, Synthesis of metallic silver nanoparticles decorated mesoporous SnO_2 for removal of methylene blue dye by coupling adsorption and photocatalytic processes, J. Photochem. Photobiol. A. Chem., 346 (2017) 77–88.
[5] F. Namvar, S. Azizi, R. Mohamad, A.B. Moghaddam, M. Soltani, F. Moshfegh, Nanosized silver–palm pollen nanocomposite, green synthesis, characterization and antimicrobial activity, Res. Chem. Intermediat., 42 (2016) 1571–1581.
[6] C. Viseras, C. Aguzzi, P. Cerezo, M.C. Bedmar, Biopolymer–clay nanocomposites for controlled drug delivery, Mater. Sci. Technol., 24(9) (2008) 1020–1026.
[7] W.M.Z.W. Yunus, N.A. Ibrahim, Synthesis and characterization of silver/clay nanocomposites by chemical reduction method, Am. J. Appl. Sci., 6(11) (2009) 1909–1914.
[8] M.B. Ahmad, M.Y. Tay, K. Shameli, M.Z. Hussein, J.J. Lim, Green synthesis and characterization of silver/chitosan/polyethylene glycol nanocomposites without any reducing agent, Int. J. Mol. Sci., 12(8) (2011) 4872–4884.
[9] U.B. Jagtap, V.A. Bapat, Green synthesis of silver nanoparticles using *Artocarpus heterophyllus Lam.* seed extract and its antibacterial activity, Ind. Crops Prod., 46 (2013) 132–137.
[10] N. Naowanat, N. Thouchprasitchai, S. Pongstabodee, Adsorption of emulsified oil from metalworking fluid on activated bleaching earth-chitosan-SDS composites: Optimization, kinetics, isotherms, J. Environ. Manage., 169 (2016) 103–115.
[11] M. Ghaedi, B. Sadeghian, A.A. Pebdani, R. Sahraei, A. Daneshfar, C. Duran, Kinetics, thermodynamics and equilibrium evaluation of direct yellow 12 removal by adsorption onto silver nanoparticles loaded activated carbon, Chem. Eng. J., 187 (2012) 133–141.
[12] H. Noyan, M. Önal, Y. Sarıkaya, The effect of sulphuric acid activation on the crystallinity, surface area, porosity, surface acidity, and bleaching power of a bentonite, Food Chem., 105(1) (2007) 156–163.
[13] A.A. Babaei, A. Khataee, E. Ahmadpour, M. Sheydaei, B. Kakavandi, Z. Alaee, Optimization of cationic dye adsorption on activated spent tea: Equilibrium, kinetics, thermodynamic and artificial neural network modeling, Korean J. Chem. Eng., 33(4) (2016) 1352–1361.
[14] N. Barka, M. Abdennouri, M.E. Makhfouk, Removal of Methylene Blue and Eriochrome Black T from aqueous solutions by biosorption on *Scolymus hispanicus L.*: Kinetics, equilibrium and thermodynamics, J. Taiwan Inst. Chem. Eng., 42(2) (2011) 320–326.
[15] G. Biçer, F. Gönen, Telon Blue AGLF Adsorption by nio-based nanomaterials: equilibrium, kinetic, and thermodynamic approach, JOTCSA, 4(3) (2017) 675–690.
[16] V.K. Gupta, D. Pathania, N.C. Kothiyal, G. Sharma, Polyaniline zirconium (IV) silicophosphate nanocomposite for remediation of methylene blue dye from waste water, J. Mol. Liq., 190 (2014) 139–145.
[17] N.N. Nassar, A. Ringsred, Rapid adsorption of methylene blue from aqueous solutions by goethite nanoadsorbents, Environ. Eng. Sci., 29(8) (2012) 790–797.
[18] L. Ai, C. Zhang, F. Liao, Y. Wang, M. Li, L. Meng, J. Jiang, Removal of methylene blue from aqueous solution with magnetite loaded multi-wall carbon nanotube: kinetic, isotherm and mechanism analysis, J. Hazard. Mater., 198 (2011) 282–290.
[19] Z. Chen, J. Zhang, J. Fu, M. Wang, X. Wang, R. Han, Q. Xu, Adsorption of methylene blue onto poly (cyclotriphosphazene-co-4, 4′-sulfonyldiphenol) nanotubes: kinetics, isotherm and thermodynamics analysis, J. Hazard. Mater., 273 (2014) 263–271.
[20] Y. Li, Q. Du, T. Liu, X. Peng, J. Wang, J. Sun, L. Xia, Comparative study of methylene blue dye adsorption onto activated carbon, graphene oxide, and carbon nanotubes, Chem. Eng. Res. Des., 91(2) (2013) 361–368.
[21] W.J. Weber Jr. J.C. Morris, Kinetics of adsorption on carbon from solution, J. Sanit. Eng. Div. Am. Soc. Civ. Eng., 89 (1963) 31–59.